General study of multipactor between curved metal surfaces

V. E. Semenov[1], J. Rasch[2], E. Rakova[1], and J. F. Johansson[3]

1) Institute of Applied Physics, Nizhny Novgorod, Russia.
2) Chalmers University of Technology, Göteborg, Sweden
3) RUAG Space AB, Göteborg, Sweden

Abstract

An analytical study of the electron trajectories between two opposite electrodes having curved surfaces is undertaken for the case when the electron transit time exceeds the rf period. The analysis is based on a statistical approach which makes it possible to calculate the width of an electron bunch after a number of electron transits taking into account the spread of electron emission velocity, and the spatial non-uniformity of the rf field using the concept of the ponderomotive force. The results are used to estimate the multipactor threshold in terms of a value of the secondary emission yield which is necessary to balance electron losses. Based on the model it is predicted that multipactor is impossible inside the realistic configuration of a helix antenna where four electrodes are placed on the same cylindrical surface.

Introduction

Multipactor is a serious failure mechanism for microwave equipment operating under vacuum conditions. The resulting electron avalanche will generate noise, detune the equipment, and may even lead to gas breakdown and system damage. Therefore multipactor prediction is an important technical problem, and when new rf equipment is designed it is standard practice to take into account the multipactor limits. Typically, accurate predictions of the multipactor threshold inside realistic rf components requires extended numerical simulations [1-3]. However, more general analytical studies can be also very useful when it is necessary to search for the components which are the best protected against multipactor. During the last decade numerical simulations of multipactor have been performed for a number of particular components including different waveguides [4-11], waveguide irises [12-13], microstrip and coaxial lines [14-18], rf filters [19-20], etc. At the same time, up to now the general multipactor theory is based on a few models which deal with electrons oscillating between two plane surfaces, or in the vicinity of one plane surface [21-24]. Very little analytical work has been done so far for the case of multipactor between curved surfaces, and so far only the case of a transmission line composed of two cylindrical wires has been considered [25]. The latter study demonstrated that the surface curvature can be responsible for defocusing of electron trajectories resulting in a considerable enhancement of the multipactor threshold. However, it is clear that if the surfaces are concave, and the surfaces are within a certain distance from each other, the opposite effect (focusing of electron trajectories) is also possible. In such a case the risk of multipactor can be increased significantly. In this paper we develop a simplified model for multipactor between two conductors having an arbitrary surface curvature. The model cannot be used to make very accurate predictions of the multipactor threshold, but it enables one to formulate general rules, and identify parameter regions where the risk of multipactor is enhanced, and reduced accordingly. Specifically the model does not describe the multipactor resonance zones in the parameter space. Its applicability is restricted mainly to systems with relatively large gaps between the electrodes, and electron transit times which considerably exceeds the rf period. In this case the resonance phenomenon is blurred by the spread of the electron emission velocity [26], and the effect of the spatial non-uniformity of the rf field on the electron trajectories can be described using the concept of the ponderomotive force [17,

27]. We apply this model to a realistic helix antenna (which is quite different from an arrangement of cylindrical wires, see Figs. 3 and 6) and it is shown that multipactor should be impossible in such a system.

Approximation of electron trajectories as straight lines perpendicular to the emission surface

A previous study of multipactor between two cylindrical wires showed that the main peculiarities of the averaged electron trajectories can be described using a very simple model within which these trajectories are treated as straight lines perpendicular to the emission surface [25]. The idea was justified by the fact that initial electron acceleration is directed along the vector of the rf electric field which is normal to the metal surface, and the model predictions were confirmed in exact numerical simulations [28]. For this reason, we start the analysis using the same idea and applying it to both convex and concave surfaces. In this section, the effect on the multipactor threshold by the focusing or defocusing of electron trajectories will be estimated and analyzed as a function of the surface curvature and the distance between the surfaces. In the next section, the model will be generalized by including the effects on the electron trajectories of: the tangential component (with respect to emission surface) of the electron emission velocity; the finite width of the metal electrodes; and the ponderomotive force, which is caused by the spatial non-uniformity of the rf electric field [17, 27].
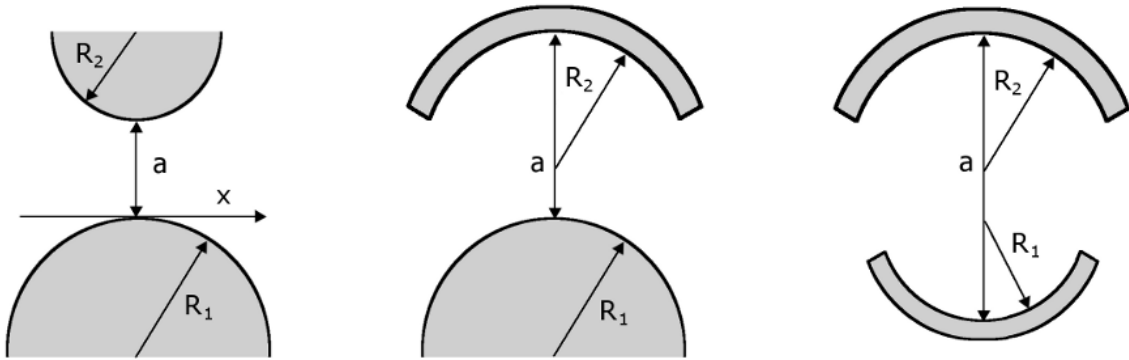
Fig. 1. Configuration of the system considered with two curved electrodes. A positive radius of curvature indicates convex surfaces (as in the figure), and a negative radius indicates a concave surface.

Consider a couple of opposing electrodes separated by a distance a, having surfaces with different radii of curvature (see Fig. 1). The system is exposed to an rf voltage, and an electron emitted from the surface of either electrode receives its first acceleration in a direction perpendicular to the electrode surface. In order to find the breakdown threshold it is only necessary to consider the case when electron losses are minimized. This corresponds to the case when $x << R$, and we shall use this assumption throughout the paper to simplify the treatment. Let an electron start from the electrode surface with some deviation, x_0, from the symmetry plane. Approximating its trajectory as straight line perpendicular to the electrode surface one can easily find the deviation, x_1, of the electron position from the symmetry plane when this electron reaches the opposite electrode:

$$x_1 = x_0 A_1 \equiv x_0 \left(1 + \frac{a}{R_1} \right), \qquad (1)$$

where A_1 is the defocusing factor for an electron transit from the first electrode to the second one, R_1 stands for the curvature radius of the first electrode ($R_1 > 0$ if this electrode is convex, $R_1 < 0$ if this electrode is concave). Assuming that each time after an impact the secondary electron starts from the impact position and using the same approximation of a straight line for its trajectory, one can calculate the deviation of the electron position after an arbitrary number of gap crossings:

$$x_{2k} = x_0 A^k, \quad x_{2k+1} = x_1 \cdot A^k, \tag{2}$$

where $A = A_1 A_2 \equiv \left(1 + \dfrac{a}{R_1}\right) \cdot \left(1 + \dfrac{a}{R_2}\right)$ plays the role of the defocusing factor for a two way electron transit. When the absolute value of this factor, A, exceeds unity (for example, in the case when both electrodes are convex) the electron trajectory is spatially unstable and its deviation from the symmetry plane increases exponentially with an increase in the number of transits. This mechanism will cause an originally small bunch of electrons to spread out during successive passages between the surfaces. In [25] it was found that the electron density evolves as $n_{2k}/n_0 = |\sigma_1 \sigma_2 / A|^k$, where n is the electron density, and σ_1 and σ_2 stand for the secondary emission yield for different one way transits. In this case the necessary condition for the multipactor avalanche to grow can be expressed as the inequality

$$\sigma = \sigma_1 \sigma_2 > |A|, \tag{3}$$

where σ denotes the effective secondary emission yield per two transits. Unless the two multipacting surfaces are similar and made of the same material σ_1 and σ_2 will not have the same value, as they depend on both impact speed and the SEY-curve. In this way, Eq. (3) can be used as a criterion for multipactor in such geometries as coaxial waveguides (see Ref [17]) and opposing cylinders of unequal radii (see Ref [25]). When one or both of the curvature radii are negative it becomes possible that $|A| \leq 1$. In this case the electron trajectories are spatially stable between the curved surfaces and a multipactor avalanche will develop provided $\sigma > 1$.
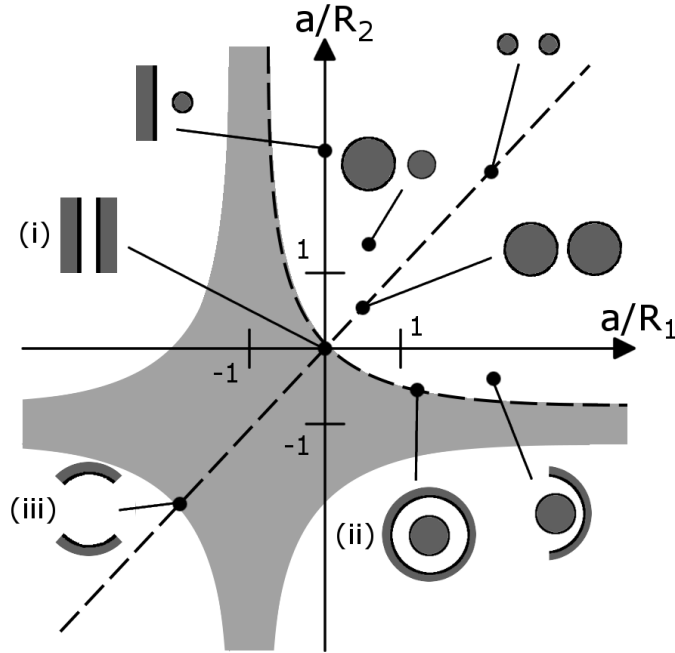
Fig. 2. A parameter chart where a range of different combinations of curvature radii are shown. The light grey area represents the region where $|A| < 1$, the curved dashed line represents all coaxial

geometries, the straight dashed line represents parallel cylinders in the upper right quadrant, and similar opposing concave surfaces in the lower left quadrant.

A summary of all the structures which can be analyzed using this simple scheme is seen in Fig. 2. Outside the grey area the geometric defocusing of electrons determines the loss rate, and the threshold is given by Eq. (3), whereas inside the grey area there is no net dilution of the electron bunches.

The simplest examples of structures where electron trajectories are spatially stable are

(i)   two parallel plane electrodes where $R_1, R_2 \rightarrow \infty$, $A = 1$ (point of origin in Fig. 2, marked by (i));

(ii)   coaxial line where $R_1 > 0, R_2 < 0, a = -R_2 - R_1, A = 1$ (points on the curved dashed line in Fig. 2, marked by (ii));

(iii)   Two electrodes covering opposite sides of the same cylindrical surface, where $R_1 = R_2 < 0, a = -R_2 - R_1, A = 1$ (the point marked by (iii) in Fig. 2).

In practice, due to the manufacturing process, the cross section of a realistic helix antenna has much more in common with the latter case (iii) (see Figs. 3 and 6) than with an arrangement of cylindrical wires, as was assumed in [25]. This means that without including the ponderomotive force in the model, no net geometric defocusing will take place, and a more accurate analysis is needed to estimate the rate of electron losses and the multipactor threshold in such a structure. This analysis is detailed in the next section where a more sophisticated model of the electron trajectories is considered, taking into account the spread of electron tangential velocities, the finite width of the electrodes, and the action of the ponderomotive force on the electron motion in a non-uniform rf field.
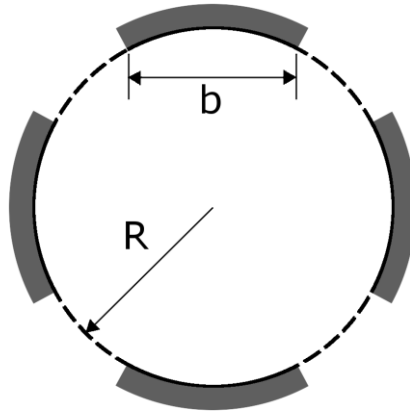
Fig. 3. Cross section of a realistic helix antenna with four electrodes placed on the same cylindrical surface.

Advanced model of the electron trajectories

The emission velocity of secondary electrons has a certain spread over angle with respect to the surface of emission. The tangential component of the emission velocity will cause electrons to deviate from the straight lines we assumed in the previous section. Furthermore, the spatial non-uniformity of the rf electric field in the gap between the two electrodes will result in a perturbation of the average electron trajectory from that of a straight line. The motion due to the non-uniformity can be described using the concept of the ponderomotive force. Typically, under multipactor conditions, the electron emission velocity is small compared to that which the electron gets due to acceleration in the rf field,

and the ponderomotive force is also relatively weak. Therefore the deviation of the trajectories from the straight line perpendicular to the emission surface is not strong and this effect can be neglected when geometrical focusing or defocusing is considerable (when the absolute value of the defocusing factor, A, is not very close to unity) as takes place in e.g. the case of multipactor between two parallel cylinders [Ref. 25]. On the other hand, when multipactor occurs in systems that are close to those listed in points (i) and (iii) above, the geometrical focusing or defocusing is weak (the defocusing factor $|A| \approx 1$) and even a small deviation of the electron trajectories from the straight line perpendicular to the emission surface can be an important effect which governs electron losses as well as the multipactor threshold.

A first order approximation of the effects of the electron emission velocity and the ponderomotive force can be performed by considering the electron trajectories that are close to the symmetry plane ($x = 0$) between the electrodes. In this case one can neglect the perturbation of the electron transit time, τ, and restrict oneself to a study of the average electron motion in a direction perpendicular to the symmetry plane (along the x-axis in Fig. 1). Due to the symmetry we can use an expansion for the electric field along the x-axis on the form

$$E(x) \approx E(0) + \frac{1}{2} x^2 \frac{\partial^2 E}{\partial x^2}\bigg|_{x=0} , \tag{4}$$

The ponderomotive force in the x-direction is given by

$$F_{p,x} = -\frac{e^2}{4m\omega^2} \frac{\partial E^2}{\partial x} , \tag{5}$$

Where $-e$, and m stand for electron charge and mass respectively, and ω is the angular field frequency. Using Eqs. (4) and (5), the electron motion along the x-direction can be described by the following equation:

$$\frac{d^2 x}{dt^2} \approx \Gamma^2 \cdot x , \tag{6}$$

where $\Gamma^2 = -\frac{1}{2}\left(\frac{e}{m\omega}\right)^2 E(0) \frac{\partial^2 E}{\partial x^2}\bigg|_{x=0}$ is assumed to be positive value (which corresponds to a

maximum of the rf field amplitude E in the symmetry plane). The dimension of Γ is s^{-1}, and Γ^{-1} represents the time-scale for considerable increase in the x-component of the average electron velocity. For the ponderomotive force to be considered weak, and for the ponderomotive concept to be applicable, it is necessary that the rate of this velocity increase is not too fast, and that the time-scale for this increase is much longer than the field period, i.e. $\Gamma << \omega$.

Due to the curvature of the emission surfaces, an electron that is emitted in the direction of the surface normal will initially gain an average velocity component in the x-direction. Since we are close to the symmetry plane, this component is approximately proportional to the deviation of the electron initial position, x_0, from the symmetry plane:

$$\dot{x}_0 \approx v_i \frac{x_0}{R} \approx \frac{a}{\tau} \frac{x_0}{R} , \tag{7}$$

where $v_i \approx a/\tau$ stands for the absolute value of the averaged electron velocity, and R is the curvature radius of the emission surface. Obviously, a nonzero tangential component, v_T, of the electron emission velocity will give an additional contribution to the initial value of the average

6

electron velocity in the x-direction. Taking this into account one should look for a solution of Eq. (6) with the following initial conditions

$$t = 0, \quad x = x_0, \quad \dot{x} = \left(ax_0 / R\tau\right) + v_T, \tag{8}$$

where $v_T \ll a/\tau$ under typical multipactor conditions. Taking for simplicity $\Gamma = \text{const.}$ and solving Eq. (6), the first coordinate of electron impact can be expressed as

$$x_1 = x_0 \cdot \left[\cosh(\Gamma\tau) + (a/R) \cdot \frac{\sinh(\Gamma\tau)}{\Gamma\tau} \right] + (v_T\tau) \cdot \frac{\sinh(\Gamma\tau)}{\Gamma\tau}, \tag{9}$$

One should note that when neglecting the ponderomotive force effect ($\Gamma \rightarrow 0$) and the tangential component of the electron emission velocity ($v_T \rightarrow 0$) this solution gives the same result as Eq. (1). When neglecting only the tangential component of the emission electron velocity, Eq. (9) simply reduces to the following modification of the defocusing factor, A,

$$A = A_1 A_2 \equiv \left[\cosh(\Gamma\tau_1) + (a/R_1) \cdot \frac{\sinh(\Gamma\tau)}{\Gamma\tau} \right] \cdot \left[\cosh(\Gamma\tau_2) + (a/R_2) \cdot \frac{\sinh(\Gamma\tau)}{\Gamma\tau} \right], \tag{10}$$

where it is taken into account that the electron transit time can be different in opposite directions, as is the case in e.g. a coaxial line [17]. Detailed calculations (see Fig. 4) show that the defocusing factors, A_1 and A_2, increase monotonously with increasing ponderomotive force and transit time. This is intuitively clear because electrons are pushed out of the region with a high rf field amplitude. In the case of convex electrodes, an increase in the defocusing factor always corresponds to an increase in the spatial instability of electron trajectories, which is accompanied by an increase both in electron losses and the multipactor threshold. However, in the case of concave electrodes, the defocusing factors can be negative. In this case the ponderomotive force can result in a decrease of the absolute value of the defocusing factor (see curve 3 in Fig. 4), which leads to the possibility of electron trajectory stabilization and thereby a decrease in the multipactor threshold. As is clear from Eq. (10), the stabilization of electron trajectories in the case of concave electrodes occurs only within a limited range of the product of the transit time and the ponderomotive force strength. A further increase of this parameter is always accompanied by the destabilization of the trajectories, and an exponential increase in the rate of electron losses (Fig. 4).
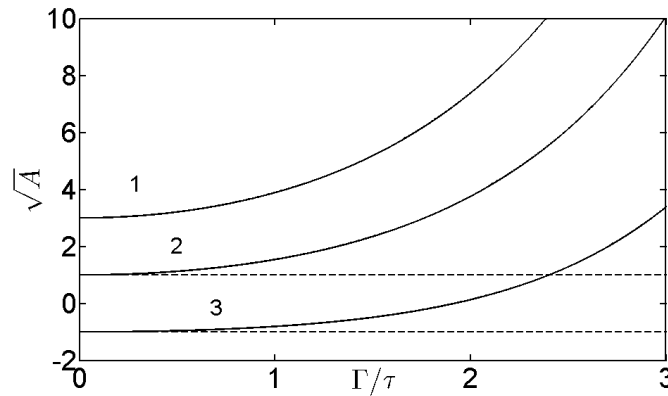
Fig. 4. The dependence of the defocusing factor per one transit on the product of the ponderomotive force and the transit time in case of similar electrodes with: convex surfaces (curve 1) with $a = 2R_1$, plane surfaces (curve 2), and concave surfaces (curve 3) with $a = -2R_1$. Between the dashed lines, the ponderomotive force serves to stabilize the electron trajectories, but as $\Gamma\tau$ becomes bigger, the ponderomotive force becomes too strong, destabilizes the trajectories, and causes the threshold to rise.

In general, the emission of an electron is a stochastic process which is associated with some spread in the electron emission velocity. This spread will also give rise to a spread in the impact position, which means that it is necessary to apply a statistical approach when analyzing Eq. (9). The tangential emission velocity can be described by some statistical distribution, $\phi(v_T)$, that is independent of the emission position on the electrode, and we assume

$$\int_{-\infty}^{\infty} \phi(v_T)dv_T = 1, \quad \langle v_T \rangle = \int_{-\infty}^{\infty} v_T \phi(v_T)dv_T = 0, \quad \langle v_T^2 \rangle = \int_{-\infty}^{\infty} v_T^2 \phi(v_T)dv_T = V_{1,2}^2 \quad (11)$$

The impact position will also follow some statistical distribution, $f_k(x_k)$, which changes upon each passage. We assume that

$$\int_{-\infty}^{\infty} f_k(x_k)dx_k = 1 \tag{12}$$

The $k+1$'th impact position, x_{k+1}, is a function of the k'th impact position, x_k, and the tangential emission velocity, v_T, and we define its average as

$$\langle x_{k+1} \rangle = \int_{-\infty}^{\infty} \int_{-\infty}^{\infty} x_{k+1}(x_k, v_T) f_k(x_k) \phi(v_T)dx_k dv_T \tag{13}$$

Within this statistical approach the main attention is paid to the average position of electron impacts, $\langle x_k \rangle$, and its variance, $D_k = \langle x_k^2 \rangle - \langle x_k \rangle^2$, after k transits. Based on these assumptions one obtains from (9) that

$$\langle x_1 \rangle = A_1 \langle x_0 \rangle, \quad D_1 = A_1^2 D_0 + B_1^2, \quad B_1 = \frac{\sinh(\Gamma \tau_1)}{\Gamma \tau_1}(V_1 \tau_1), \tag{14}$$

where $\langle x_0 \rangle$ and D_0 are the average position and variance of the first electron bunch respectively. Performing similar calculations to a sequence of electron transits results in

$$\langle x_{2k} \rangle = A^k \langle x_0 \rangle, \quad \langle x_{2k+1} \rangle = A^k \langle x_1 \rangle, \tag{15}$$

$$D_{2k} = A^{2k}(D_0 - G_1) + G_1, \quad D_{2k+1} = A^{2k}(D_1 - G_2) + G_2, \tag{16}$$

where the defocusing factors A_1, A_2, A are defined in (10) and

$$G_1 = \frac{A_2^2 B_1^2 + B_2^2}{1 - A^2}, \quad G_2 = \frac{A_1^2 B_2^2 + B_1^2}{1 - A^2}, \quad B_2 = \frac{\sinh(\Gamma \tau_2)}{\Gamma \tau_2}(V_2 \tau_2), \tag{17}$$

As follows from (15), the average deviation of the electron impact position from the symmetry plane is governed by the defocusing factors, which are independent on the spread of the electron emission velocity. Equation (16) makes it possible to formulate explicitly a criterion for the multipactor threshold in terms of the electron bunch half-width, $\Delta_k = \sqrt{D_k}$. It should be noted that the electron bunch will have no clear outer boundary, which means that any definition of the bunch width will be somewhat arbitrary. When the absolute value of the defocusing factor, A, exceeds unity, the spatial instability of the electron trajectories results in an exponential growth of this width with an increasing number of transits, and the inequality (3) should be fulfilled to balance the growth of the width to ensure an increase in the electron density. As was mentioned above, the defocusing factor does not depend on the spread of the electron emission velocity. However (as can be seen from Eq. (16)) the spread of the electron emission velocity guarantees a nonzero width of the electron bunch even in the case of a single seed electron starting exactly at $x = 0$. In the latter case the initial average coordinate and variance of the electron bunch are zero ($\langle x_0 \rangle = 0$, $D_0 = 0$) and the solutions (15)-(16) can be rewritten as

$$\langle x_k \rangle = 0, \tag{18}$$

$$D_{2k} = \frac{1 - A^{2k}}{1 - A^2}\left(A_2^2 B_1^2 + B_2^2\right), \quad D_{2k+1} = A^{2k}B_1^2 + \frac{1 - A^{2k}}{1 - A^2}\left(A_1^2 B_2^2 + B_1^2\right), \tag{19}$$

It can be seen from Eq. (19) that in the case of spatially unstable electron trajectories ($A^2 > 1$), the spread of electron emission velocity triggers an exponential increase in the electron bunch width ($D_{2k} \propto A^{2(k-1)}$, when $k \to \infty$). Since the electron bunch starts with a zero width, the electron emission velocity spread is necessary to start the increase in the bunch width, but once that process is started, the velocity spread plays a minor part in the further dispersion of the electron bunch, and the threshold for multipactor is mainly set by the geometrical conditions (which includes the ponderomotive effect). But in the case when the trajectory is spatially stable the electron emission velocity spread can be responsible for considerable increase in the multipactor threshold. Specifically, when the absolute value of all defocusing factors approach unity (this takes place when e.g. the action of the ponderomotive force is neglected between two plane parallel electrodes or between electrodes covering opposite sides of the same cylindrical surface) the solution (19) describes a linear increase of the variance with the number of transits:

$$D_{2k} \cong k\left(B_1^2 + B_2^2\right), \quad \text{if} \quad A_1^2 \to 1 \text{ and } A_2^2 \to 1, \tag{20}$$

This corresponds to an unlimited growth of the electron bunch width, which will exceed the width of the electrodes after a number of transits. As a result, there will be electron losses over the electrode edges, and the multipactor threshold will increase. In the case when $A^2 < 1$ the spread of the electron emission velocity makes an unlimited decrease of the electron bunch width impossible. And as $k \to \infty$ the bunch half-width instead approaches the finite limit

$$\Delta_{2k} = \sqrt{D_{2k}} = \frac{1}{\sqrt{1 - A^2}}\sqrt{A_2^2 B_1^2 + B_2^2}, \quad \Delta_{2k+1} = \frac{1}{\sqrt{1 - A^2}}\sqrt{A_1^2 B_2^2 + B_1^2} \tag{21}$$

If this limit exceeds half the electrode width the multipactor threshold will increase due to the electron losses, despite the fact that the electron trajectories are spatially stable, see Fig. 5.
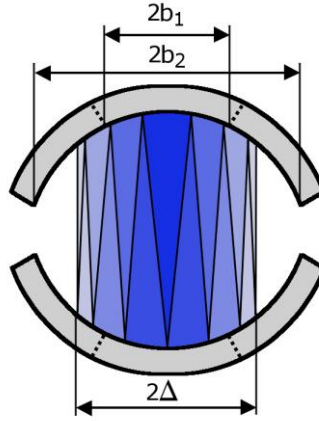
Fig. 5. An illustration of the growth of the width of an electron bunch (the blue regions) between successive impacts on the electrodes (grey regions). In the case when $A^2 < 1$ the electron bunch width approaches a certain value 2Δ, if this width is smaller than the electrode widths ($b_2 > \Delta$) no electron losses due to geometry will occur. On the other hand, when the electrodes are smaller than the bunch width ($b_1 < \Delta$), there will be electron losses over the edge of the electrodes.

9

Effect of finite electrode width on the multipactor threshold

When geometrical spreading is strong it is sufficient to consider the evolution of the electron density, and use Eq. (3) as a criteria for breakdown. However, in systems where the electron bunch width approaches a finite value it is instead necessary to consider the losses of electrons over the conductor edges. This leads to a modified breakdown criteria, where we require exponential growth in the total number of electrons involved in the discharge for multipactor to be possible. In the case of finite electrode widths a simple estimate of the multipactor threshold can be derived by considering a sequence of electron transits after the moment when the electron bunch width, 2Δ, have grown to equal the electrode width, $2b$. We can define an enhancement factor, η_k, which is simply the number of secondary electrons generated in an impact divided by the number of impacting electrons. For the case when an electron transit is completed with $\Delta_k < b_{1,2}$ it seems reasonable to assume that no electrons are lost over the electrode edges. In this case the enhancement factor is simply equal to the secondary emission yield, i.e. $\eta_k = \sigma_k$, and the secondary electron bunch will start on the opposite electrode with the same width as it had at impact. On the other hand, each time an electron transit is finished with $\Delta_k > b_{1,2}$ one can assume that a fraction, $1 - \dfrac{b_{1,2}}{\Delta_k}$, of the electrons is lost, in which case the enhancement electron factor will equal $\eta_k = \sigma_k \dfrac{b_{1,2}}{\Delta_k}$, and the secondary electron bunch will start from the opposite electrode with a width equal to that of the electrode. In a sequence of transits the electron enhancement factor is multiplied, and the condition for the electron number to grow, and a multipactor avalanche to develop, can be expressed as the following inequality

$$\prod \eta_k > 1, \tag{22}$$

This condition is simplified considerably when both electrodes have identical parameters ($R_1 = R_2 = R$, $b_1 = b_2 = b$, $\tau_1 = \tau_2 = \tau$, $V_1 = V_2 = V$, $\sigma_1 = \sigma_2 = \sigma$). In this case, after achieving equality between the electron bunch width and the electrode width, all subsequent electron transits will be identical, and all electron enhancement factors, η_k, will be the same. Based on the solution (14) one can find the value of η_k and express the necessary condition for a multipactor avalanche to develop as the following inequalities:

$$\sigma > \sqrt{\left[\cosh(\Gamma\tau) + \frac{a}{R}\frac{\sinh(\Gamma\tau)}{\Gamma\tau}\right]^2 + \left[\frac{\sinh(\Gamma\tau)}{\Gamma\tau}\right]^2 \left(\frac{V\tau}{b}\right)^2}, \tag{23}$$

if the RHS of (23) exceeds unity or

$$\sigma > 1, \tag{24}$$

if the RHS of (23) is lower than unity (in this case the electron bunch width will never exceed the electrode width if the bunch starts from a single seed electron at $x = 0$).

The two summands under the square root on the RHS of Eq. (23) represent separate contributions from different effects into the enhancement of the multipactor threshold. The first term represents the contribution of the surface curvature and the ponderomotive force. It depends on neither electron emission velocity nor electrode width. When this term is taken alone it gives the previous estimate (3) for the multipactor threshold with the defocusing factor defined in (10). The second term represents the contribution of the electron emission velocity, which is enhanced by the action of the ponderomotive force. This term is independent on the surface curvature.

Application of the model to some particular cases.

Applying the simplified model above to some particular structures makes it possible to get a better understanding of a number of previously published results. Specifically, taking (23) with $\Gamma = 0$ and

$(a/R) = 0$ one immediately finds the multipactor threshold, $\sigma > \sqrt{1 + \left(\dfrac{V\tau}{b} \right)^2}$, previously obtained in

[12] for a waveguide iris using the approximation of a uniform rf field. If we wish to make a more accurate estimate of the multipactor threshold within an iris by applying our model, we need to find an approximation for the second derivative of the electric field. Since the conductors have the half-width b , a rough estimate should be

$$\left. \frac{\partial^2 E}{\partial x^2} \right|_{x=0} \approx -\frac{E_0}{b^2}, \qquad (25)$$

where E_0 stands for the maximum of the rf field amplitude. This makes it possible to to express the

product $\Gamma\tau$ via pure geometrical parameters based on the approximation $\tau = \dfrac{a}{V_\omega}$, where $V_\omega = \dfrac{eE_0}{m\omega}$

stands for the electron oscillatory velocity. This approximation for the crossing time is based on two assumptions for the drift velocity of the electrons. First of all one assumes that the drift velocity is

maximal, i.e. $V_i \approx V_\omega + V_N$ [26](see Eq. (7)), where $V_N = \sqrt{\langle v_N^2 \rangle}$ is a statistical average of the

emission velocity in the direction of the surface normal. Under typical multipactor conditions this is generally true, and one can also use $V_\omega >> V_N$, leading to $V_i \approx V_\omega$. Secondly one assumes that the drift velocity of the electrons is constant during the passage over the gap. This assumption was justified in [26], where it was shown that between two cylindrical conductors, the maximum drift

velocity is $\sqrt{\dfrac{3}{2}} V_\omega$, which results in only a minor correction to the estimate $\tau = \dfrac{a}{V_\omega}$. Using these

assumptions we find

$$(\Gamma\tau) \approx \frac{a}{\sqrt{2}b}, \qquad (26)$$

Substituting this estimate of the ponderomotive force into (23) the multipactor threshold for an iris can be expressed as

$$\sigma > \sqrt{\cosh^2 \left(\frac{a}{\sqrt{2}b} \right) + 2 \left(\frac{V}{V_\omega} \right)^2 \sinh^2 \left(\frac{a}{\sqrt{2}b} \right)}, \qquad (27)$$

which is in qualitatively agreement with the main features of the simulation results obtained in [13]. As was mentioned above, under typical multipactor conditions the electron initial velocity is small compared to that one which electron achieve due to acceleration in rf field ($V << V_\omega$). Therefore the estimate (27) explicitly illustrates that inside an iris with $a/b \geq 1$ the contribution of the ponderomotive force into the enhancement of the multipactor threshold is more important than the contribution of the electron emission velocity spread.

Applying a similar approximation, $\left. \dfrac{\partial^2 E}{\partial x^2} \right|_{x=0} \approx -\dfrac{E_0}{R^2}$, for the rf field non-uniformity in a

system with two parallel cylinders of equal radii, as in [25], one finds an estimate of the multipactor threshold as

11

$$\sigma > \sqrt{\left[\cosh\left(\frac{a}{\sqrt{2}R}\right) + \sqrt{2}\sinh\left(\frac{a}{\sqrt{2}R}\right)\right]^2 + 2\left(\frac{V}{V_\omega}\right)^2 \sinh^2\left(\frac{a}{\sqrt{2}R}\right)}, \tag{28}$$

This result justifies one in neglecting the contribution of the electron emission velocity spread into the multipactor threshold enhancement, which was done in [25]. At the same time it follows from (28) that for a large distance between the wires, the contribution of the ponderomotive force into the multipactor threshold enhancement (which was neglected in [25]) can be very important. In deriving Eq. (28) we assumed that $b = R$, which means that we violated the condition $x << R$. Eq. (28) can therefore not be considered as an exact result, but rather an underestimation of the real threshold.

In the case of two opposite electrodes placed on the same cylindrical surface (see Figs. 3 and 6), the radii of curvature are the same and negative, $R_1 = R_2 = -|R|$, whereas the distance between the electrodes is $a = 2|R|$. Therefore taking the approximations (25)-(26) the defocusing factors are estimated to be

$$A_1 = A_2 = \cosh\left(\sqrt{2}R/b\right) - \sqrt{2}\frac{\sinh\left(\sqrt{2}R/b\right)}{(R/b)}, \tag{29}$$

Due to the manufacturing process, many helix antennas have such geometries, see Fig. 6.

Fig. 6. Quadrifilar helix antenna for X-band (c. 8 GHz). Photo: RUAG Space AB.

One particular example of a helix antenna which is used commercially for communication at 400 MHz has the dimensions $|R| = 4$ cm, and $b = 4$ mm. In this case the defocusing factors are so high ($A_1 \approx 6 \times 10^5$) that a multipactor avalanche becomes completely impossible between one pair of electrodes. However a realistic helix antenna with a cross section like that in Figs. 3 and 6 contains two pairs of electrodes, and an electrons which is pushed out of the gap between one pair has a certain probability to impact an electrode of the second pair. In the case of a very high defocusing factor (when $A_1 >> 2\pi|R|/b$) an electron which is emitted from one electrode will suffer a major deflection during transit, which will cause it to miss the opposing electrode, and it is unclear exactly where it will end up. For a very conservative estimate of what kind of losses this infers we assume that the electron can reach almost any point of the cylinder surface with uniform probability. In this case the probability to impact any of the other electrodes is estimated to be

$$P_{imp} \approx \frac{6b}{2\pi|R| - 2b}, \tag{30}$$

For the parameters of the 400 MHz commercial antenna this probability is, $P_{imp} \approx 0.1$. Therefore, in this case, electron losses can be balanced, and the multipactor avalanche can grow, if and only if the secondary emission yield exceeds the threshold value

$$\sigma > \sigma_{th} = P_{imp}^{-1} \approx 10, \tag{31}$$

This threshold seems to be unrealistically high for clean metal surfaces, and it should be possible to state that the realistic helix antenna should be multipactor free.

Conclusion

We have developed a simple model for estimating the multipactor threshold in a gap between two electrodes having curves surfaces. The model is based on a statistical analysis of the electron bunch width after a number of the gap transits. The consideration is based on an approximate approach to the calculation of electron trajectories averaged over the rf period. This approximation is valid when the electron transit time exceeds the rf period, and makes it possible to take into account the electron dispersion due to the electron emission velocity spread, the surface curvature, and the effect of spatial non-uniformity of the rf field. The model is applied to some particular systems (waveguide iris and two wire transmission line) which makes it possible to compare the results with those published previously, and achieve a better understanding of the main effects responsible for the enhancement of the multipactor threshold. When applying the model to the realistic structure of a helix antenna, the model predicts that multipactor is impossible due to effect of the ponderomotive force which pushes electrons out of the regions with strong rf field.

References

1. J. de Lara, F. Pérez, M. Alfonseca, L. Galán, I. Montero, E. Román, and D. Raboso, *Multipactor Prediction for On-Board Spacecraft RF Equipment with the MEST Software Tool*. IEEE Trans. Plasma Sci., **34**, 2, pp. 476-484 (2006).

2. M. Yu, *Power-Handling Capability for RF Filters*, IEEE Microwave Magazine, **8**, 5, pp. 88-97 (2007).

3. M. Jiménez, B. G. Martínez, D. Raboso, S. Anza, A. Álvarez, F. Quesada, V. E. Boria, C. Vicente, and J. Gil, *Multimodal Characterization of the Multipactor Effect in Microwave Waveguide Components*, IEEE Microwave and Wireless Components Letters, **22**, 2, pp. 61-63 (2012).

4. V. E. Semenov, E. I. Rakova, D. Anderson, M. Lisak, and J. Puech, *Multipactor in rectangular waveguides*, Phys. Plasmas, **14**, 033501, pp. 1-8 (2007).

5. I. A. Kossyi, G. S. Lukyanchikov, V. E. Semenov, E. I. Rakova, D. Anderson, M. Lisak, and J. Puech, *Polyphase (non-resonant) multipactor in rectangular waveguides*, J. Phys. D: Appl. Phys., **41,** 065203, pp 1-8 (2008).

6. A. M. Pérez, V. E. Boria, B. Gimeno, S. Anza, C. Vicente, and J. Gil. *Multipactor Analysis in Circular Waveguides,* J. Electromagn. Waves Appl., **23**, 11-12, pp. 1575-1583 (2009).

7. V. E. Semenov, N. A. Zharova, D. Anderson, M. Lisak, and J. Puech, *Simulations of Multipactor in Circular Waveguides*, Phys. Plasmas, **17**, 123503, pp. 1-7 (2010).

8. V. Semenov, E. Rakova, N. Zharova, D. Anderson, M. Lisak, and J. Puech, *Simulations of the Multipactor Effect in Hollow Waveguides with Wedge-Shaped Cross Section*, IEEE Trans. Plasma Sci., **36**, 2, 488-493 (2008).

9. J. Hueso, C. Vicente, B. Gimeno, V. E. Boria, S. Marini, and M. Taroncher, *Multipactor Effect Analysis and Design Rules for Wedge-Shaped Hollow Waveguides*, IEEE Trans. Elec. Dev., **57**, 12, pp. 3508-3517 (2010).

10. A. Frotanpour, G. Dadashzadeh, M. Shahabadi, and B. Gimeno, *Analysis of Multipactor RF Breakdown Thresholds in Elliptical Waveguides*, IEEE Trans. Elec. Dev., **58**, 3, pp. 876-881 (2011).

11. D. González-Iglesias, P. Soto, S. Anza, B. Gimeno, V. E. Boria, C. Vicente, and J. Gil. *Multipactor Susceptibility Charts for Ridge and Multiridge Waveguides*, IEEE Trans. Elec. Dev., **59**, 12, pp. 3601-3607 (2012).

12. R. Udiljak, D. Anderson, M. Lisak, J. Puech, and V. E. Semenov, *Multipactor in a Waveguide Iris*, IEEE Trans. Plasma Sci., **35**, 2, pp. 388-395 (2007).

13. V. E. Semenov, E. Rakova, R. Udiljak, D. Anderson, M. Lisak, and J. Puech, *Conformal mapping analysis of multipactor breakdown in waveguide irises,* Phys. Plasmas **15**, 033501, pp. 1-8 (2008).

14. V. E. Semenov, E. I. Rakova, A. G. Sazontov, I. M. Nefedov, V. I. Pozdnyakova, I. A. Shereshevskii, D. Anderson, M. Lisak and J. Puech, *Simulations of multipactor thresholds in shielded microstrip lines,* J. Phys. D: Appl. Phys., **42,** 205204, pp 1-7 (2009).

15. S. K. Nagesh, D. Revannasiddiah, and S. V. K. Shastry, *Investigation of multipactor breakdown in communication satellite microwave co-axial systems,* PRAMANA – J. Phys., Indian Academy of Sciences, **64**, 1, pp. 95-110 (2005).

16. A. M. Perez, C. Tienda, C. Vicente, S. Anza, J. Gil, B. Gimeno, V. E. Boria, and D. Raboso, *Prediction of Multipactor Breakdown Thresholds in Coaxial Transmission Lines for Travelling, Standing, and Mixed Waves*, IEEE Trans. Plasma Sci., **37**, 10, pp. 2031-2040 (2009).

17. R. Udiljak, D. Anderson, M. Lisak, V. E. Semenov, and J. Puech*, Multipactor in a coaxial transmission line. I. Analytical study*. Phys. Plasmas, **14**, 033508, pp. 1-11 (2007).

18. V. E. Semenov, N. Zharova, R. Udiljak, D. Anderson, M. Lisak, and J. Puech*, Multipactor in a coaxial transmission line. II. Particle-in-cell simulations*, Phys. Plasmas, **14**, 033509, pp. 1-7 (2007).

19. C. Vicente, M. Mattes, D. Wolk, B. Mottet, H. L. Hartnagel, J. R. Mosig, and D. Raboso, *Multipactor Breakdown Prediction in Rectangular Waveguide Based Components*, IEEE MTT-S Int. Microwave Symp. Dig., pp. 1055-1058 (2005).

20. I. Arregui, S. Anza, I. Arnedo, C. Vicente, A. Lujambio, J. Gil, M. Chudzik, B. Gimeno, T. Lopetegi, M. A. G. Laso, and V. E. Boria, *Multipactor prediction in novel high-power low-pass filters with wide rejection band*, Proc. Microwave Conf., EuMC 2009, Rome, Sept. 29 - Oct. 1, 2009, pp. 675 – 678.

21. H. C. Kim, and J. P. Verboncoeur, *Time-dependent physics of a single-surface multipactor discharge*, Phys. Plasmas, **12**, 123504, pp. 1-7 (2005).

22. A. Sazontov, V. Semenov, M. Buyanova, N. Vdovicheva, D. Anderson, M. Lisak, J. Puech, and L. Lapierre, *Multipactor Discharge on a Dielectric Surface: Statistical Theory and Simulation Results,* Phys. Plasmas, **12**, 093501, pp. 1-7 (2005).

23. A. G. Sazontov, and V. E. Nechaev, *Effects of rf magnetic field and wave reflection on multipactor discharge on a dielectric*, Phys. Plasmas, **17**, 033509, pp. 1-10 (2010).

24. G. Cheng, and L. Liu, *Temporal Evolution of Multipactor Electron Discharge on a Dielectric Under Excitation of High-Power Microwave*, IEEE Trans. Plasma Sci., **39**, 4, pp. 1067-1074 (2011).

25. J. Rasch, D. Anderson, J. F. Johansson, M. Lisak, J. Puech, E. Rakova, and V. E. Semenov, *Microwave Multipactor Breakdown Between Two Cylinders*, IEEE Trans. Plasma Sci., **38**, 8, pp. 1997-2005 (2010).

26. A. Kryazhev, M. Buyanova, V. Semenov, D. Anderson, M. Lisak, J. Puech, L. Lapierre, and J. Sombrin, *Hybrid resonant modes of two-sided multipactor and transition to the polyphase regime*, Phys. Plasmas, **9**, 11, p. 4736-4743 (2002).

27. A. V. Gaponov, and M. A. Miller, *Potential Wells for Charged Particles in a High-Frequency Electromagnetic Field*, Sov. Phys. JETP, **7**, pp. 168-169 (1958). Original publication: Zhurnal Eksperimental'noi i Teoreticheskoi Fiziki, **34**, 1, p 242-243 (1958).

28. J. Rasch, V. E. Semenov, E. Rakova, D. Anderson, J. F. Johansson, M. Lisak, and J. Puech, *Simulations of Multipactor Breakdown Between Two Cylinders*, IEEE Trans. Plasma Sci., **39**, 9, pp. 1786-1794 (2011).